Nanoparticle-induced twist-grain boundary phase

Maja Trček,[1] George Cordoyiannis,[1,2,*] Vassilios Tzitzios,[3] Samo Kralj,[4] George Nounesis,[3]
Ioannis Lelidis,[2] and Zdravko Kutnjak[1,5]

[1]*Condensed Matter Physics Department, Jožef Stefan Institute, 1000 Ljubljana, Slovenia*
[2]*Department of Physics, National and Kapodistrian University of Athens, 15784 Zografou, Greece*
[3]*Biomolecular Physics Laboratory, National Centre for Scientific Research "Demokritos," 15310 Aghia Paraskevi, Greece*
[4]*Faculty of Natural Sciences and Mathematics, University of Maribor, 2000 Maribor, Slovenia*
[5]*Jožef Stefan International Postgraduate School, 1000 Ljubljana, Slovenia*

(Received 17 December 2013; published 2 September 2014)

By means of high-resolution ac calorimetry and polarizing optical microscopy, it is demonstrated that surface-functionalized spherical CdSSe nanoparticles induce a twist-grain boundary phase when dispersed in a chiral liquid crystal. These nanoparticles can effectively stabilize the one-dimensional lattice of screw dislocations, thus establishing the twist-grain boundary order between the cholesteric and the smectic-*A* phases. A Landau–de Gennes–Ginzburg model is used to analyze the impact of nanoparticles on widening the temperature range of molecular organizations possessing a lattice of screw dislocations. We show that in addition to the defect-core-replacement mechanism, the saddle-splay elasticity may also play a significant role.

DOI: 10.1103/PhysRevE.90.032501 PACS number(s): 61.30.Jf, 61.30.Mp, 64.70.M−

I. INTRODUCTION

The existence of twist-grain boundary phases (TGBs) was theoretically predicted as the liquid-crystalline analog of the Shubnikov phase exhibiting Abrikosov flux vortices in type-II superconductors [1,2]. An isomorphism was proposed between liquid crystals and superconductors as follows: chiral nematic phase (N^*), normal metal, twisted chiral line liquid (N_L^*), Abrikosov vortex liquid, twist-grain boundary *A* (TGB_A), Abrikosov vortex lattice, smectic-*A* (Sm*A*), Meissner phase [3]. TGBs were experimentally discovered by Goodby *et al.* [4] and Nguyen *et al.* [5]. Since then, they have been identified in pure liquid crystals (LCs) as well as mixtures of LCs and chiral dopants [3,6]. Their thermal signatures [7], x-ray patterns [8,9], nuclear magnetic resonance spectra [10,11], and optical textures [12] have been repeatedly established. TGB_A phase consists of a one-dimensional lattice of screw dislocations along the grain boundaries that separate slabs of smectic-*A* order. This defect lattice is pinned for TGB_A, whereas it strongly oscillates in the case of N_L^* phase [13] leading to only short-range TGB order.

Various types of nanoparticles have been often dispersed in liquid crystals in order to study the effects or quenched-random disorder on phase transitions [14–18], explore memory effects [19], tailor the dielectric and optical properties [20–22], and stabilize blue phases [23–25]. Very recently, it has been reported that the same surface-functionalized nanoparticles (NPs) that are crucial for blue phase stabilization [26], can also induce TGB_A and N_L^* phases in a chiral liquid-crystal compound [27] that does not exhibit TGB ordering in its pure form. This compound is CE6 [4′-(2-methylbutyl)phenyl-4-decyloxybenzoate], and the nanoparticles used in the study were CdSe quantum dots with a 3.5-nm diameter, surface-treated with oleyl amine (OA) and tri-octyl phosphine (TOP). So far, it has not been demonstrated whether the nanoparticle-induced TGB order is system specific or it can be encountered in a wider variety of chiral LCs and nanoparticles. Thus, in our present work, we explore the possible induction of TGB_A and N_L^* phases in another chiral LC that is substantially different from CE6. This is the compound 4′-octyl-biphenyl-4-carboxylic acid 4-(2-methyl-butyl)-phenyl ester (CE8) exhibiting a very different phase sequence than CE6 [27] albeit with the chiral nematic (N^*)–smectic-*A* (Sm*A*) phase transition. Notably, CE8 was the first compound where the dispersion of (OA+TOP)-treated quantum dots resulted in the widening of the blue phase III temperature range by almost a tenfold. We have also opted to modify the spherical nanoparticles used in Ref. [24] and have synthesized CdSSe quantum dots that favor a higher concentration of OA on their surface. Our experimental results obtained by means of high-resolution ac calorimetry and polarizing optical microscopy establish the induction of TGB_A order in CE8 and clearly distinguish between the optical textures of N_L^* and TGB_A phases characterized by the short- and long-range TGB orders, respectively. To explain the general character of the observed properties of the mixtures, a theoretical model is also included in the paper that describes the impact of nanoparticles on the widening of phases possessing a one-dimensional lattice of screw dislocations. We show that, in addition to the trapping of NPs and the replacement of the defect core [27], the saddle-splay elasticity is also important in explaining the widening of the TGB phases due to the dispersion of nanoparticles.

II. SAMPLES AND EXPERIMENTAL METHODS

The high-purity chiral liquid crystal CE8 was purchased from Merck and it was used without any additional treatment. The CdS_xSe_{1-x} NPs have been synthesized in N.C.S.R. "Demokritos" for $x = 0.5$. Atomic force microscopy measurements, performed at Jožef Stefan Institute, yield a diameter value of 3.4 ± 0.3 nm as shown in Fig. 1. This diameter distribution is analogous to what was used in [24] for the CdSe quantum dots. The surface of NPs is treated with flexible chains of OA and TOP. Such a coating has been proven very effective for homogeneous dispersion of various types of spherical or

*Corresponding author: george.cordoyiannis@ijs.si

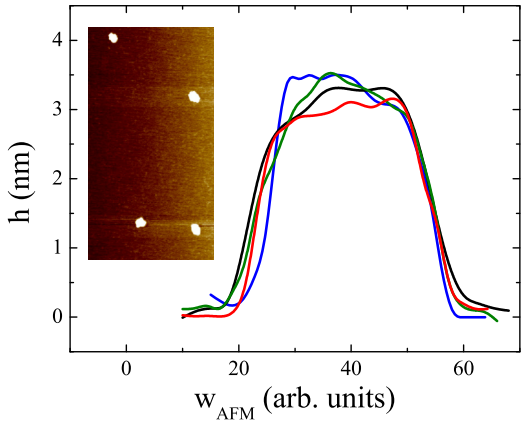

FIG. 1. (Color online) Atomic force microscopy measurements yield a diameter of 3.4 ± 0.3 nm for the CdSSe NPs.

anisotropic NPs in liquid-crystal hosts [24,26–29]. For the CdSSe NPs, though, the presence of S is expected to yield a higher concentration of OA molecules at the surface, relatively to their CdSe counterparts, since TOP binds preferentially only upon Se while OA upon Cd and S.

Two mixtures with CdSSe concentration of $\chi = 0.01$ and 0.05 have been prepared, where χ is defined as the mass of NPs over the total mass of the sample, i.e., $\chi = m_{\mathrm{NP}}/(m_{\mathrm{LC}} + m_{\mathrm{NP}})$. For the mixture preparation, a well-established protocol used in previous studies [24,30] has been followed. This protocol includes the use of an ultrasonic bath to break any aggregates in the NPs solution, persistent mixing by magnetic stirring at elevated temperatures, and, finally, stirring and drying under vacuum in order to remove any solvent remains. Afterwards, the samples were loaded into high-purity silver cells for calorimetric measurements and between glass plates treated for planar anchoring of the liquid-crystal molecules, for microscopic observations. Prior to any data acquisition, they were heated for a short period of time (5 min) to temperatures corresponding to the isotropic phase of pure CE8. The temperature profiles of heat capacity for pure CE8 and the two mixtures with CdSSe nanoparticles have been obtained using a fully computerized, high-resolution ac calorimeter at Jožef Stefan Institute. This apparatus operates in the conventional ac as well as in relaxation (or nonadiabatic scanning) mode. The ac mode is mainly sensitive to continuous enthalpy changes, whereas an anomalous or continuous behavior for the temperature profile of the phase of the ac temperature oscillations indicates whether a transition is first or second order, respectively. The relaxation mode, on the other hand, is sensitive to both continuous and discontinuous (latent heat) enthalpy changes. The comparison of the data between the two modes of operation can provide a quantitative determination of the latent heat. A detailed description of the apparatus is given in Ref. [31]. At any given temperature, the heat capacity of the empty cell was subtracted in order to obtain the net specific heat capacity (C_p) of the samples. All the samples were additionally observed under a Carl Zeiss Jena microscope. The samples were placed between glass plates separated by 20 μm spacers. These plates are coated with a unidirectionally rubbed polyimide, thus, imposing planar anchoring conditions to the LC molecules. The images were captured under cross polarizers. The temperature was stabilized and slowly changed with a rate of 3 K/h by means of a homemade heating stage, with a temperature stability of ±10 mK.

III. EXPERIMENTAL RESULTS AND DISCUSSION

Pure CE8 exhibits a sharp peak at 406.4 K associated with a direct, weakly first order N^*-SmA phase transition [24]. Interestingly, a low-temperature shoulder also appears at the low-temperature wing of the heat capacity anomaly at approximately 0.2 K lower than the main peak (Fig. 2). Relatively to pure CE8, the $\chi = 0.01$ and 0.05 mixtures exhibit a substantially different thermal behavior. First, as shown by the cooling runs with a rate of 0.25 Kh^{-1} in Fig. 2, the heat capacity anomalies are smeared and broadened due to the presence of the CdSSe NPs. Second, the low-temperature wings of the C_p anomalies reveal additional smeared thermal features, suggesting the presence of new phase(s) between the N^* and the SmA. In order to more accurately probe the shape of these additional peaks, subsequent heating runs were performed using a significantly slower scanning rate of 0.15 Kh^{-1}. These heating runs revealed the presence of two small but clearly distinct anomalies (shown in Fig. 2 top panel)

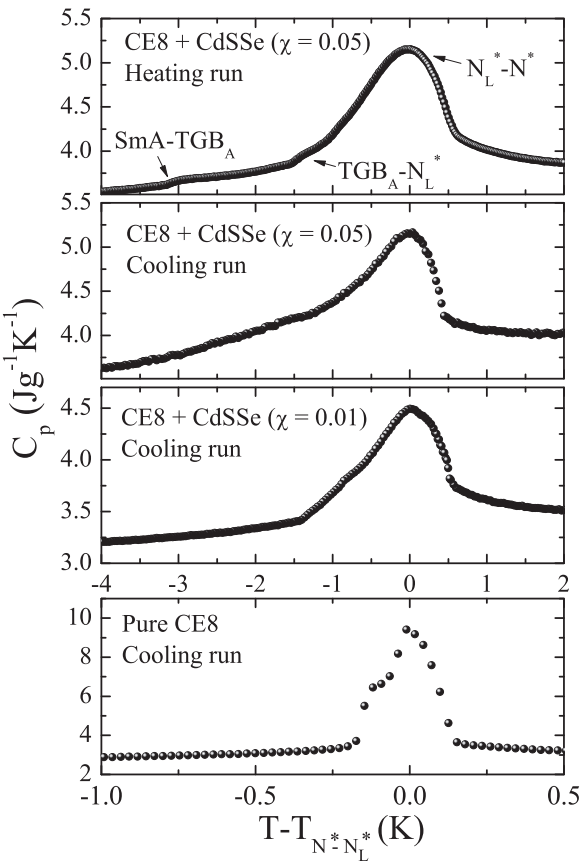

FIG. 2. The $C_p(T)$ profiles for pure CE8 as well as for the $\chi = 0.01$ and 0.05 mixtures, upon cooling with a rate of 0.25 Kh^{-1} and heating (only the $\chi = 0.05$ mixture is shown) with a rate of 0.15 Kh^{-1}. In all cases, the low-temperature wings of the peaks display additional features. In the case of the two mixtures, these features correspond to the characteristic thermal pattern of SmA-TGB$_A$-N_L^*-N^* phase sequence [7,27].

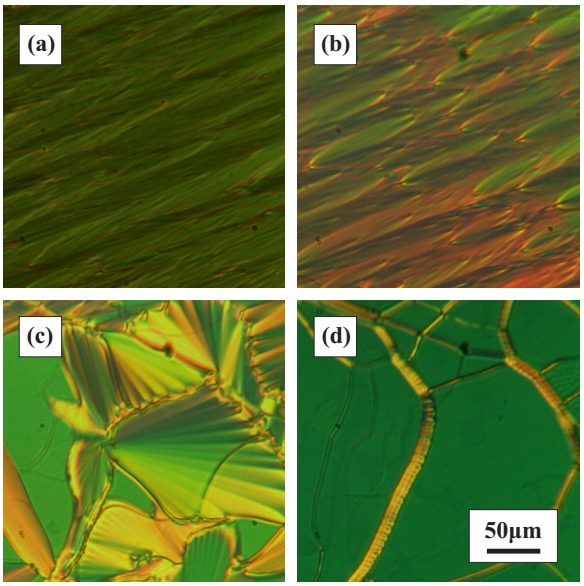

FIG. 3. (Color online) Polarizing optical microscopy textures upon heating the $\chi = 0.05$ sample from the SmA phase; (a) SmA, (b) TGB$_A$, (c) N_L^*, and (d) N^* phase. The images have been obtained under crossed polarizers.

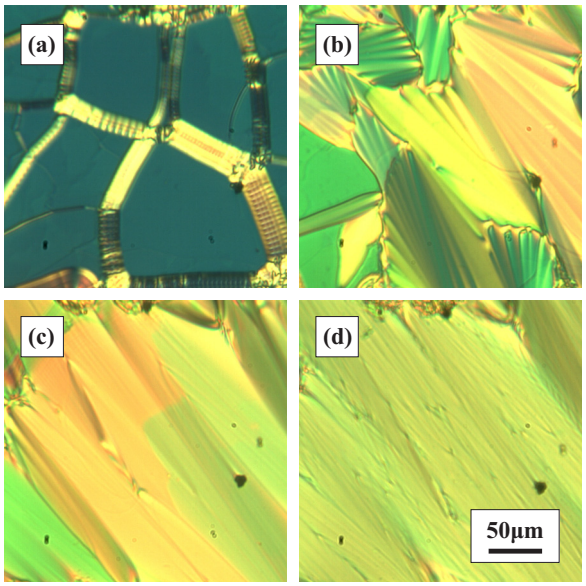

FIG. 4. (Color online) Polarizing optical microscopy textures upon cooling the $\chi = 0.05$ sample from the N^* phase; (a) N^*, (b) N_L^*, (c) TGB$_A$, and (d) SmA phase. The images have been obtained under crossed polarizers.

corresponding to the typical pattern of a SmA-TGB$_A$-N_L^*-N^* phase sequence [7]. Note that for systems composed of LC + NPs, these additional anomalies, attributed to the SmA-TGB$_A$ and TGB$_A$-N_L^* phase transitions, appear more rounded [27] compared to the ones observed in pure liquid crystals [7]. Especially, the TGB$_A$-N_L^* peak may not really describe a phase transition but a supercritical transformation where the long-range TGB order becomes only short range in the N_L^* phase. It is certainly interesting to note that the peak characterized with maximum enthalpy is for the N_L^*-N^* transition, which involves the short-range establishment of the grain boundaries.

Searching for additional experimental proof about the presence of the TGB$_A$ and N_L^* phases, the $\chi = 0.01$ and 0.05 mixtures were observed under the microscope upon slow heating and cooling. Apart from the well-oriented SmA domains and the oily streaks characteristic of the N^* phase, two intermediate textures have been identified and they could be attributed to the TGB$_A$ and N_L^* structures. These textures can be seen in Fig. 3 for heating and in Fig. 4 for cooling. In case of heating, for TGB$_A$ the texture is similar with the one of SmA phase, although it becomes more colorful due to the continuous rotation of the smectic slabs. In addition, the elongated SmA fans are progressively attaining rounded edges. The fans become essentially wider and attain stripes along the next appearing N_L^* phase and finally change to the oily streaks in the N^* phase. Similar to the heating runs, the subsequent cooling runs reproduced nicely these four different textures. Since the calorimetric profiles and especially those for heating scans clearly distinguish a sequence of four different phases, the observed optical microscopy textures can thus be attributed to the aforementioned phases. To our knowledge, no other study has so far distinguished between the optical textures of TGB$_A$ and N_L^* structures. In the case of pure CE8, our optical microscopy measurements also detect textures that can be associated to TGB$_A$ order, in agreement with the low-temperature calorimetric shoulder observed in the heat capacity anomaly. The stability of the TGB$_A$-like texture was found to be dependent upon the anchoring strength for planar alignment of the LC molecules. It would thus appear that pure CE8 may be very close to a N^*-TGB$_A$-SmA triple point. Indeed, a likely optical microscopy observation of a very narrow-ranged TGB$_A$ phase has been previously reported [33]. The temperature range of TGB order, derived by calorimetric and optical microscopy measurements upon heating and cooling, is presented on Table I. This range includes both the short- and long-range TGB orders, i.e., the total temperature range of N_L^* and TGB$_A$ phases.

The results obtained by both high-resolution calorimetry and microscopy demonstrate that the dispersion of CdSSe NPs can induce TGB order in a narrow temperature range between the N^* and SmA phases of CE8. The effect has been briefly described by means of an *adaptive-defect-core-targeting* (ADCT) mechanism [27] for the system CE6 + CdSe NPs. The basis of ADCT is the so-called *defect-core-replacement* (DCR) mechanism [32] combined with the adaptive character of NPs with respect to the surrounding LC ordering. In the following section, the NP-induced stabilization of TGB order is discussed. Here, the possible contribution of

TABLE I. The temperature range of TGB order (ΔT_{TGB}) as a function of NPs concentration (χ) is presented here, upon heating and cooling.

χ	$\Delta T_{\mathrm{TGB}}^{(\mathrm{heating})}$ (K)	$\Delta T_{\mathrm{TGB}}^{(\mathrm{cooling})}$ (K)
0 (pure CE8)	0.2	0.2
0.01	1.7	1.4
0.05	3.0	3.2

saddle-splay elasticity has been taken into account in addition to the ADCT mechanism, something that was not addressed in Ref. [27].

IV. THEORY

A simple Landau–de Gennes–Ginzburg mesoscopic approach has been used to estimate the conditions under which NPs stabilize LC structures exhibiting a lattice of screw dislocations. The local orientational ordering is determined by the headless nematic director field $\vec{n}$ and the translational ordering by the complex order parameter $\psi = \eta e^{i\phi}$. The amplitude η determines the degree of smectic ordering and the phase factor ϕ reveals the position of smectic layers. In our recent work [27] we have demonstrated the strong impact of the DCR mechanism on the stabilization of topological defects either in orientational or translational degrees of freedom. It is attributed to the reduction of relatively costly condensation free energy penalty, by partially replacing the defect core with the nonsingular volume of a trapped nanoparticle. This mechanism is efficient if NPs do not significantly disrupt the defect core structure. In this contribution, we show that the saddle-splay elasticity might also play a significant role. In the following, we illustrate the impact of these two mechanisms on the stabilization of screw dislocations, emphasizing the role of the saddle-splay mechanism. Additional details of the theoretical methodology are presented in the Appendix.

A. Free energy

The free energy density of the system $F = \int f d^3\vec{r} + \int f_i d^2\vec{r}$ consists of the volume and interface contributions. The first integral is performed over the LC body and the second one over the enclosing interface (i.e., the surfaces confining LC and NP-LC interfaces). The volume free energy density is commonly expressed as $f = f_c^{(s)} + f_e^{(n)} + f_e^{(s)}$. Here, $f_c^{(s)}$ stands for the smectic condensation contribution, and $f_e^{(s)}$ and $f_e^{(n)}$ describe the smectic and nematic elastic penalties, respectively. We neglect the interface contribution f_i describing interaction between NP and surrounding LC phase because we assume NPs to be adaptive [27]. The structure of the remaining terms is as follows [34]:

$$f_e^{(n)} = \frac{K_1}{2}(\vec{\nabla}\cdot\vec{n})^2 + \frac{K_2}{2}[\vec{n}\cdot(\vec{\nabla}\times\vec{n}) - q_{ch}]^2 + \frac{K_3}{2}|\vec{n}\times\vec{\nabla}\times\vec{n}|^2 - \frac{K_{24}}{2}\vec{\nabla}\cdot[\vec{n}(\vec{\nabla}\cdot\vec{n}) + \vec{n}\times\vec{\nabla}\times\vec{n}], \quad (1)$$

$$f_c^{(s)} = \alpha_0(T - T^*)|\psi|^2 - \beta|\psi|^4 + \gamma|\psi|^6, \quad (2)$$

$$f_e^{(s)} = C_\parallel|(\vec{n}\cdot\vec{\nabla} - iq_0)\psi|^2 + C_\perp|(\vec{n}\times\vec{\nabla})\psi|^2. \quad (3)$$

In these terms, only the most essential contributions are included in order to estimate the observed phase transition behavior. The nematic Frank elastic constants K_1, K_2, K_3, and K_{24} in the nematic elastic free energy density determine the relative costs of splay, twist, bend, and saddle-splay deformations in $\vec{n}$, respectively. The quantity q_{ch} stands for the chirality-enforced wave vector. In the smectic condensation term we have included terms up to sixth order in ψ in order to take into account a first order phase transition between SmA and N^* phase in the absence of NPs. The material constants α_0, β, γ are assumed to be independent of temperature, and T^* describes the nematic supercooling temperature for the case $q_{ch} = 0$. The elasticity of smectic layers is determined by the smectic compressibility ($C_\parallel$) and bend ($C_\perp$) elastic constant. These constants are positive in the SmA phase and enforce a one-dimensional SmA layering characterized by the layer thickness $d = 2\pi/q_0$, where the layer normal points along $\vec{n}$. The volume contribution of the saddle-splay term could be expressed as a "surface" term using the Gauss theorem. Furthermore, this term is proportional to the Gaussian curvature $G = 1/(R_1R_2)$ of a hypothetical surface whose local normal points along $\vec{n}$. Here, R_1 and R_2 determine local principal curvature radia of the surface [34]. Usually, the contribution of this term is negligible, either because one of the principal curvatures is close to zero at the "surface" or its contribution is overwhelmed by the interface interactions described by f_i.

Note that the nematic elastic constants K_2 and K_3 exhibit an anomalous increasing on approaching the smectic phase ordering by reducing temperature. This effective increase is due to the fluctuation-triggered formation of clusters exhibiting local layering, which strongly resist to the imposed bend or twist nematic director field distortions. However, in the smectic phase the smectic elasticity is dominantly described by the smectic elastic constants. Therefore, the values of the Frank nematic elastic constants are in presence of smectic layers comparable to the values deep in the nematic phase. Additionally note that within the mean-field description, we do not distinguish between the TGB$_A$ and N_L^* phase. The TGB$_A$ structure is characterized by a well-defined lattice of screw dislocations. On the contrary, in the N_L^* phase the dislocations strongly oscillate. However, the key mechanisms responsible for stabilization of defect lattices are sensitive to the topological defect core structure. The latter is similar in TGB$_A$ and N_L^* phases. Consequently, we henceforth use the former configuration as the representative defect structure.

B. Geometry of the problem

The main geometric features of the TGB$_A$ phase are shown in Fig. 5. It consists of slabs of length l_b exhibiting essentially bulk SmA ordering. These slabs are separated by grain boundaries (GB) of width comparable to the nematic penetrations length λ [34]. Within each GB, a lattice of screw dislocations resides; these dislocations are separated by a distance $l_d \sim l_b$ [3]. The presence of dislocations enables tilt between adjacent slabs, giving rise to a global twisting of the LC structure along the z axis of the coordinate frame. The volume of a representative TGB$_A$ unit cell, consisting of a SmA slab and a GB of surface l^2, is equal to $V_u \sim l_b l^2$. The length of each screw dislocation is estimated by l and their number within a GB is given by $N_{\mathrm{scr}} \sim l/l_d$.

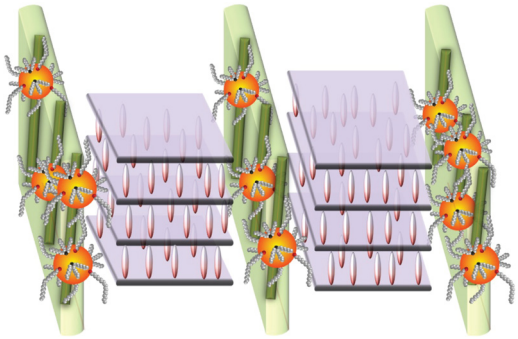

FIG. 5. (Color online) A simple schematic illustration of the CdSSe NPs trapped in the screw dislocations is shown here.

V. SCREW DISLOCATION STABILIZATION MECHANISMS

Let us suppose that NPs of concentration χ are added to a LC sample exhibiting TGB_A ordering. If they are present in LC regions where smectic ordering exists, they would dilate the smectic layers. Long-range forces would be established due to the spatially distorted smectic phase ϕ, representing the gauge component of the order parameter ψ [27]. Consequently, the NPs are predominantly assembled within the cores of screw dislocations, where the smectic ordering is essentially melted. Furthermore, due to their flexible tails, the NPs disturb relatively weakly the local orientational LC ordering. NPs trapped within cores of screw dislocations stabilize the latter by the following two key mechanisms. First, they decrease the condensation free energy penalty due to the DCR mechanism. Namely, the condensation free energy penalty $\Delta F_c^{(\mathrm{TGB})}$ due to presence of essentially smectic melted regions within cores of screw dislocations in absence of NPs is estimated by $\Delta F_c^{(\mathrm{TGB})}(\chi = 0) \sim |f_c^{(s)}(\eta_s)|(V_{\mathrm{LC}} - V_{\mathrm{scr}}^{(\mathrm{tot})})$. Here, η_s stands for the equilibrium value of smectic ordering in absence of dislocations, V_{LC} is the volume of the LC body, and $V_{\mathrm{scr}}^{(\mathrm{tot})}$ estimates the total volume of smectic melted regions due to screw dislocations. If the NPs are trapped within the cores, the condensation free energy is decreased:

$$F_c^{(\mathrm{TGB})}(\chi) = F_c^{(\mathrm{TGB})}(0) - \left|f_c^{(s)}(\eta_s)\right| V_{\mathrm{NP}}^{(\mathrm{tot})}. \quad (4)$$

Here, $V_{\mathrm{NP}}^{(\mathrm{tot})}$ describes the total volume occupied by NPs trapped within dislocations. Furthermore, the presence of NPs introduces interfaces where the saddle-splay contributions might be significant. Indeed, the director field variations along a radial direction from the center of an isolated screw dislocation exhibits a configuration [35] reminiscent to the *double twist distortion* within double twist cylinders forming blue phases [3]. The corresponding saddle-splay contribution ΔF_{24} of a single nanoparticle trapped within a core of dislocations reads as

$$\Delta F_{24} = -\frac{K_{24}}{2}\int (\vec{n} \times \vec{\nabla} \times \vec{n}) \cdot \vec{e}\, d^2\vec{r}, \quad (5)$$

where $\vec{n} \times \vec{\nabla} \times \vec{n}$ displays significant variations within the core of screw dislocation [35]. The integration is carried out over the NP-LC interface where the unit vector $\vec{e}$ describes its outer surface normal. Consequently, in the presence of NPs, the stability range of TGB_A phase is increased to a finite temperature interval that can be estimated by

$$\Delta T_{\mathrm{TGB}_A}(\chi) \sim \left(T_{NA}^{(0)} - T^*\right)\frac{\chi\rho_{\mathrm{LC}}}{\rho_{\mathrm{NPs}}}\left(1 + \frac{a_{24}}{q_{ch}^2 r d}\right)\frac{l_b^2}{\pi\xi^2}, \quad (6)$$

where the detailed derivation is given in the Appendix. Here, $T_{NA}^{(0)}$ and T^* stand for the N^*-SmA phase transition temperature and the nematic supercooling temperature for the case $q_{ch} = 0$, respectively, ρ_{NP} and ρ_{LC} stand for the mass densities of NPs and LC, ξ estimates the smectic order parameter correlation length, and r stands for the characteristic linear size of a nanoparticle. The dimensionless quantity a_{24} is estimated by

$$1/a_{24} \sim 4\pi^2[1 + 1/(4\pi r^2/d^2)]^2(r/d)^3. \quad (7)$$

In this estimate, we assumed that for $\chi = 0$ the triple point condition is realized where N^*, TGB_A, and SmA ordering coexist in order to simplify the derivation. Note that this condition seems to be realized in a similar sample using CE6 LC, as our recent study [27] suggests. By neglecting the contribution of the K_{24} term and by setting $\rho_{\mathrm{LC}}/\rho_{\mathrm{NPs}} \sim 1, l_b \sim 20$ nm, $\xi \sim 2$ nm, $T_{NA}^{(0)} - T^* \sim 1$ K, one gets for $\chi = 0.05$ an estimate $\Delta T_{\mathrm{TGB}_A}(\chi) \sim 1$ K. A finite value of K_{24} could further increase the TGB_A temperature range.

VI. CONCLUSIONS

This study has shown that the TGB_A and N_L^* phases can be induced by dispersing surface-functionalized CdSSe NPs, of a 3.5 nm diameter, in the liquid crystal CE8. Given the recent observation of NP-induced TGB_A and N_L^* phases in a system of LC + NPs where both the LC and the NPs are different [27], it is suggested that this phenomenon exhibits a more universal character. In order to identify the key mechanisms enabling significant widening of the temperature stability window of structures exhibiting a lattice of screw dislocations, a Landau–de Gennes–Ginzburg mesoscopic model has been used. Our analysis indicates that, in addition to the defect-core-replacement mechanism, the saddle-splay elasticity might also play an important role. Both mechanisms depend on the characteristic size of NPs, therefore, size is expected to have a particularly strong impact upon the stabilization of TGB phases. We anticipate that further research can unravel the precise role of NPs size and shape on inducing TGB order in chiral liquid crystals. Indicatively, our recent preliminary results show that larger anisotropic NPs with similar surface treatment do not induce any TGB order in CE8.

ACKNOWLEDGMENTS

M.T. acknowledges the support of the Project No. PR-05015 of the Slovenian Research Agency. G.C. acknowledges the support of the Project No. PE3-1535 implemented within the framework of the Action "Supporting Postdoctoral Researchers" and V.T and G.N. acknowledge support and funding by the THALES Program No. 380170 of the Operational Project "Education and Lifelong Learning," co-financed by the European Social Fund and the State of Greece. Z.K. acknowledges support from the Center of Excellence "NAMASTE" and Project No. P1-0125 of the Slovenian Research

Agency. Z.K., G.C., and S.K. acknowledge the support of the European Office of Aerospace Research and Development Grant No. FA8655-12-1-2068. I.L. acknowledges the Special Account for Research Grants of the National and Kapodistrian University of Athens for support. S.K. acknowledges the hospitality of the Isaac Newton Institute for Mathematical Sciences, Cambridge, UK, within the program "Mathematics of Liquid Crystals." We would like to thank C.W. Garland for useful discussions during the preparation of this manuscript.

APPENDIX

In this Appendix, the derivation of the impact of adaptive NPs on the stabilization of screw dislocations is given. We suppose that on average $N_{\rm NP}$ nanoparticles of volume $v_{\rm NP}$ are present within the volume V_u of a smectic slab within the TGB$_A$ phase. The average volume fraction p of NPs is then given by

$$p = (N_{\rm NP} v_{\rm NP})/V_u \sim \chi(\rho_{\rm LC}/\rho_{\rm NPs}), \tag{A1}$$

where $\rho_{\rm NP}$ and $\rho_{\rm LC}$ stand for the mass densities of NPs and LC, respectively. The LC orientational ordering within the Cartesian coordinate frame defined by the unit vector triad $\{\vec{e}_x, \vec{e}_y, \vec{e}_z\}$ is parametrized by

$$\vec{n} = \sin\theta_\parallel \sin\theta_\perp \vec{e}_x + \sin\theta_\parallel \cos\theta_\perp \vec{e}_y + \cos\theta_\parallel \vec{e}_z. \tag{A2}$$

For the sake of simplicity, we henceforth neglect the LC elastic anisotropy and set $C \equiv C_\parallel \sim C_\perp$ and $K \equiv K_1 \sim K_2 \sim K_3 \sim K_{24}$. The most important material-imposed lengths are the cholesteric pitch wavelength $P = 2\pi/q_{ch}$, the equilibrium smectic layer spacing $d = 2\pi/q_0$, the smectic order parameter correlation length ξ, and the nematic twist penetration length λ. In the following, we label the free energy costs of a phase within a unit cell V_u by $\Delta F^{(\rm phase)}$. The corresponding average free energy density is given by $f^{(\rm phase)} = \Delta F^{(\rm phase)}/V_u$.

1. Pure samples

First, the case of pure LC (without NPs) is considered. The ordering within N^* is determined by $\theta_\perp = q_{ch} z$, $\theta_\parallel = \pi/2$, and $\eta = 0$. The corresponding spatially averaged free energy density $f^{(\rm phase)} = \Delta F^{(\rm phase)}/V_u$ equals

$$f^{(N^*)} = 0. \tag{A3}$$

We describe the SmA ordering within a unit cell for $T < T_*$ by $\vec{n} = \vec{e}_x$ and $\psi = \eta_s e^{iq_0 x}$. For the first order character of the N-SmA phase transition for $q_{ch} = 0$ taking place at $T = T_{NA}^{(0)}$ the condensation free energy below $T_{NA}^{(0)}$ reads as $f_c^{(s)} = \alpha_0(T_{NA}^{(0)} - T^*)\eta_0^2[\tilde{\eta}^2(1-\Delta t) - 2\tilde{\eta}^4 + \tilde{\eta}^6] \sim -\alpha_0(T_{NA}^{(0)} - T^*)\eta_0^2 \Delta t$. Here, $\tilde{\eta} = \eta/\eta_0$, $\eta_0 = \eta(T = T_{NA}^{(0)})$,

$$\Delta t = \left(T_{NA}^{(0)} - T\right)/\left(T_{NA}^{(0)} - T^*\right). \tag{A4}$$

Accordingly,

$$f^{(\rm SmA)} = -\alpha_0\left(T_{NA}^{(0)} - T^*\right)\eta_0^2 \Delta t + \frac{K q_{ch}^2}{2}. \tag{A5}$$

In the estimation of the free energy costs for the formation of TGB$_A$ structure it is assumed that an ideal SmA ordering is established within the smectic blocks. Across each GB of width $\sim \lambda$ the director field is approximately rotated by an angle [3]

$$\Delta\theta_\perp \sim \frac{d}{l_d} \sim \frac{d}{l_b}, \tag{A6}$$

and $\theta_\parallel = \pi/2$. The elastic contribution due to distortions in $\vec{n}$ reads as

$$\int_0^{l_b} dz[\vec{n} \cdot (\vec{\nabla} \times \vec{n}) - q_{ch}]^2 \sim \frac{\Delta\theta_\perp^2}{\lambda} - 2q_{ch}\Delta\theta_\perp + q_{ch}^2 l_b.$$

A global twisting of the LC configuration is enabled by GBs incorporating a lattice of parallel screw line dislocations. The core-size radius of each dislocation is approximated by ξ and within the cores the smectic ordering is essentially melted. The resulting average smectic condensation free energy within V_u is given by

$$\Delta F_c^{(\rm TGB)} = -\alpha_0\left(T_{NA}^{(0)} - T^*\right)\eta_0^2 \Delta t (V_u - V_{\rm scr}). \tag{A7}$$

Here, $V_{\rm scr} \sim N_{\rm scr} l \pi \xi^2 \sim \pi l^2 \xi^2 / l_b$ is the volume occupied by the cores of screw dislocations. The other elastic contributions as well as the interactions among dislocations are not considered [36]. Note that this approximation works well only in the limit $l_d \gg \lambda$. It follows

$$f^{(\rm TGB)} = \frac{K}{2}\left(\frac{\Delta\theta_\perp^2}{\lambda l_b} - \frac{2q_{ch}\Delta\theta_\perp}{l_b} + q_{ch}^2\right) - \alpha_0(T_{NA}^{(0)} - T^*)\eta_0^2 \Delta t\left(1 - \frac{\pi\xi^2}{l_b^2}\right). \tag{A8}$$

Our previous study using CE8 LC reveals that in the absence of NPs, the phase exhibiting screw dislocations is not present, whereas it appears if even a minute amount of NPs is added. This suggests that in pure samples the triple point condition is roughly established. In order to simplify the estimate for the NP-driven enhancement of the temperature interval of TGB$_A$ phase stability, we set that similar conditions are also realized in the case of CE6 LC. Therefore, we set that at the direct N^*-SmA phase transition (at $T = T_{NA}$), all the competing phases coexist, therefore $f^{(\rm TGB)}(T_{NA}) = f^{(N^*)}(T_{NA}) = f^{(\rm SmA)}(T_{NA})$. Consequently, at the triple point it holds

$$T_{NA} \sim T_{NA}^{(0)} - \frac{\left(T_{NA}^{(0)} - T^*\right)}{2}(\lambda\xi q_0 q_{ch})^2, \tag{A9}$$

where we estimated the nematic penetration length and order parameter correlation length by $\lambda \sim \sqrt{K/(C\eta_0^2 q_0^2)}$ and $\xi \sim \sqrt{C/\alpha_0(T_{NA}^{(0)} - T^*)}$, respectively. The critical value of the chirality wave vector enabling the triple point condition at $T = T_{NA}$ reads as

$$q_{ch}^{(c)} \sim \frac{d}{\pi\xi^2}\left(1 - \sqrt{1 - \frac{\pi\xi^2}{\lambda l_b}}\right). \tag{A10}$$

Therefore, the absence of chirality corresponds to an infinite value for l_b.

2. Samples with NPs

Next, it is assumed that NPs of an average volume concentration p are added [see Eq. (A1)]. It is assumed

that NPs are predominantly assembled within the cores of dislocations. Consequently, they decrease the condensation free energy penalty which is required to introduce topological defects. Furthermore, due to their flexible tails, the NPs disturb relatively weakly the local LC ordering. The corresponding main free energy penalties in the translational degree of order read as

$$\Delta F_c^{(\mathrm{TGB})} = -\alpha_0\big(T_{NA}^{(0)} - T^*\big)\eta_0^2\Delta t(V_u - V_{\mathrm{scr}} + N_{\mathrm{NP}}v_{\mathrm{NP}}). \tag{A11}$$

Next, we take into account the saddle-splay contribution $\Delta F_{24}^{(\mathrm{TGB})} = -\frac{K_{24}N_{\mathrm{NP}}}{2}\int(\vec{n}\times\vec{\nabla}\times\vec{n})\cdot\vec{e}\,d^2\vec{r}$, where the integral is performed over the NP-LC interface. In the local cylindrical coordinate system attached to a screw dislocation defined by a unit vector triad $\{\vec{e}_\rho, \vec{e}_\varphi, \vec{e}_z\}$, where the center of cylindrically symmetric dislocation is placed at $\rho = 0$, the director field can be well parametrized by $\vec{n} \sim \cos\vartheta\,\vec{e}_z + \sin\vartheta\,\vec{e}_\varphi$. It holds $\vec{n}(\rho = 0) = \vec{e}_z$ and in the limit $\rho/d \gg 1$ the director distribution is well described by [35]

$$\vartheta = \arctan[1/(\rho q_0)]. \tag{A12}$$

Taking into account Eq. (A12), we obtain an estimate

$$\frac{\Delta F_{24}^{(\mathrm{TGB})}}{V_u} \sim -\frac{Kpa_{24}}{2rd}, \tag{A13}$$

where r stands for the characteristic linear size of NP and the dimensionless quantity a_{24} is given by Eq. (7). Note that this expression is approximate. Here, the most important information is that the saddle-splay term yields a finite contribution if a NP is trapped within a screw dislocation. Therefore, in the presence of NPs it holds

$$f^{(\mathrm{TGB})}(p) \sim f^{(\mathrm{TGB})}(0) - p\left(\alpha_0\big(T_{NA}^{(0)} - T^*\big)\eta_0^2\Delta t + \frac{Ka_{24}}{2rd}\right), \tag{A14}$$

while the impact of NPs on the other two phases is much smaller. From relation $f^{(\mathrm{TGB})}(p) = f^{(\mathrm{Sm}A)}$ it follows

$$\begin{aligned}\Delta T_{\mathrm{TGB}_A}(\chi) &= T_{NA} - T_{\mathrm{TGB}}(\chi)\\ &\sim \big(T_{NA}^{(0)} - T^*\big)p\left(1 + \frac{a_{24}}{q_{ch}^2 rd}\right)\frac{l_b^2}{\pi\xi^2},\end{aligned} \tag{A15}$$

which is equivalent to Eq. (6).

[1] P. G. de Gennes, Solid State Commun. **10**, 753 (1972).
[2] S. R. Renn and T. C. Lubensky, Phys. Rev. A **38**, 2132 (1988).
[3] H. S. Kitzerow, in *The Physics of Liquid Crystals,* edited by H. S. Kitzerow and C. Bahr (Springer, New York, 2001).
[4] J. W. Goodby, M. A. Waugh, S. M. Stein, E. Chin, R. Pindak, and J. S. Patel, Nature (London) **337**, 449 (1989).
[5] H. T. Nguyen, A. Bouchta, L. Navailles, P. Barois, N. Isaert, R. J. Twieg, A. Maaroufi, and C. Destrade, J. Phys. II **2**, 1889 (1992).
[6] J. Fernsler, L. Hough, R. F. Shao, J. E. Maclennan, L. Navailles, M. Brunet, N. V. Madhusudana, O. Mondain-Monval, C. Boyer, J. Zasadzinski *et al.*, Proc. Natl. Acad. Sci. USA **102**, 14191 (2005).
[7] T. Chan, C. W. Garland, and H. T. Nguyen, Phys. Rev. E **52**, 5000 (1995).
[8] L. Navailles, P. Barois, and H. T. Nguyen, Phys. Rev. Lett. **71**, 545 (1993).
[9] L. Navailles, B. Pansu, L. Gorre-Talini, and H. T. Nguyen, Phys. Rev. Lett. **81**, 4168 (1998).
[10] V. Domenici, C. A. Veracini, V. Novotná, and R. Y. Dong, Chem. Phys. Chem. **9**, 556 (2008).
[11] T. Apih, V. Domenici, A. Gradišek, V. Hamplová, M. Kaspar, P. J. Sebastião, and M. Vilfan, J. Phys. Chem. B **114**, 11993 (2010).
[12] I. Dierking and S. T. Lagerwall, Liq. Cryst. **26**, 83 (1999).
[13] D. R. Nelson and H. S. Seung, Phys. Rev. B **39**, 9153 (1989).
[14] T. Bellini, L. Radzihovsky, J. Toner, and N. A. Clark, Science **294**, 1074 (2001).
[15] M. Marinelli, A. K. Ghosh, and F. Mercuri, Phys. Rev. E **63**, 061713 (2001).
[16] P. S. Clegg, C. Stock, R. J. Birgeneau, C. W. Garland, A. Roshi, and G. S. Iannacchione, Phys. Rev. E **67**, 021703 (2003).
[17] G. Cordoyiannis, G. Nounesis, V. Bobnar, S. Kralj, and Z. Kutnjak, Phys. Rev. Lett. **94**, 027801 (2005).
[18] G. Cordoyiannis, L. K. Kurihara, L. J. Martínez-Miranda, C. Glorieux, and J. Thoen, Phys. Rev. E **79**, 011702 (2009).
[19] S. Relaix, R. L. Leheny, L. Reven, and M. Sutton, Phys. Rev. E **84**, 061705 (2011).
[20] Y. Reznikov, O. Buchnev, O. Tereshchenko, V. Reshetnyak, and A. Glushchenko, Appl. Phys. Lett. **82**, 1917 (2003).
[21] J. P. F. Lagerwall and G. Scalia, J. Mater. Chem. **18**, 2890 (2008).
[22] R. Basu and G. S. Iannacchione, Phys. Rev. E **81**, 051705 (2010).
[23] H. Yoshida, Y. Tanaka, K. Kawamoto, H. Kubo, T. Tsuda, A. Fujii, S. Kuwabata, H. Kikuchi, and M. Ozaki, Appl. Phys. Express **2**, 121501 (2009).
[24] E. Karatairi, B. Rožič, Z. Kutnjak, V. Tzitzios, G. Nounesis, G. Cordoyiannis, J. Thoen, C. Glorieux, and S. Kralj, Phys. Rev. E **81**, 041703 (2010).
[25] I. Dierking, W. Blenkhorn, E. Credland, W. Drake, R. Kociuruba, B. Kayser, and T. Michael, Soft Matter **8**, 4355 (2012).
[26] G. Cordoyiannis, P. Losada-Pérez, C. S. P. Tripathi, B. Rožič, U. Tkalec, V. Tzitzios, E. Karatairi, G. Nounesis, Z. Kutnjak, I. Muševič *et al.*, Liq. Cryst. **37**, 1419 (2010).
[27] G. Cordoyiannis, V. S. R. Jampani, S. Dhara, S. Kralj, V. Tzitzios, G. Basina, G. Nounesis, Z. Kutnjak, C. S. P. Tripathi, P. Losada-Pérez *et al.*, Soft Matter **9**, 3956 (2013).
[28] M. Lavrič, G. Cordoyiannis, S. Kralj, V. Tzitzios, G. Nounesis, and Z. Kutnjak, Appl. Opt. **52**, E47 (2013).
[29] M. Lavrič, V. Tzitzios, S. Kralj, G. Cordoyiannis, I. Lelidis, G. Nounesis, V. Georgakilas, H. Amenitsch, A. Zidanšek, and Z. Kutnjak, Appl. Phys. Lett. **103**, 143116 (2013).
[30] H. Haga and C. W. Garland, Phys. Rev. E **56**, 3044 (1997).
[31] H. Yao, K. Ema, and C. W. Garland, Rev. Sci. Instrum. **69**, 172 (1998).

[32] H. Kikuchi, M. Yokota, Y. Hisakado, H. Yang, and T. Kajiyama, Nat. Mater. **1**, 64 (2002).
[33] P. Wilson, S. Cowling, and D. Lacey, 8th International Conference on Ferroelectric Liquid Crystals (P2-70), Washington DC, 2001 (unpublished).
[34] M. Kléman and O. D. Lavrentovich, *Soft Matter Physics* (Springer, Berlin, 2003).
[35] S. Kralj and T. J. Sluckin, Phys. Rev. E **48**, R3244 (1993).
[36] I. Lelidis, C. Blanc, and M. Kléman, Phys. Rev. E **74**, 051710 (2006).